Interseismic coupling and asperity distribution along the Kamchatka subduction zone

Roland Bürgmann,[1] Mikhail G. Kogan,[2] Grigory M. Steblov,[3] George Hilley,[1,4] Vasily E. Levin,[5] and Edwin Apel[1]

Received 27 January 2005; revised 18 March 2005; accepted 6 April 2005; published 19 July 2005.

[1] GPS measurements of interseismic horizontal surface velocities reveal the degree of kinematic coupling of the plate boundary thrust along the Kamchatka subduction zone from about 51° to 57°N latitude. Inversions for the distribution of aseismic slip rate along the ~15°NW dipping underthrust suggest a nonslipping plate interface in southern Kamchatka above ~50 km depth, along the segment that ruptured in the M_w = 9, 1952 earthquake. North of ~53°N, the subduction interface experiences significant aseismic slip, consistent with the lower seismic moment release in $M \leq 8.5$ earthquakes along this portion of the subduction zone. The GPS velocities are consistent with a boundary element forward model in which historic earthquake rupture zones are represented as locked asperities, surrounded by a zero shear stress subduction interface loaded by plate convergence. Models in which the complete rupture zones of historic earthquakes are considered locked greatly overpredict the degree of kinematic coupling. Reducing the area of the locked model asperities to the central 25% area of historic rupture zones fits the data well, suggesting that large earthquakes involve small fully locked core asperities surrounded by conditionally stable portions of the plate interface. Areas of low aseismic slip rate appear to be roughly correlated with areas of low isostatic gravity anomalies over offshore forearc basins, while less coupled portions of the Kamchatka subduction zone coincide with high-gravity anomalies offshore of two peninsulas, possibly related to the subduction of the Emperor-Meji seamount chain and the Kruzenstern fracture zone.

Citation: Bürgmann, R., M. G. Kogan, G. M. Steblov, G. Hilley, V. E. Levin, and E. Apel (2005), Interseismic coupling and asperity distribution along the Kamchatka subduction zone, *J. Geophys. Res.*, *110*, B07405, doi:10.1029/2005JB003648.

1. Introduction

[2] Subduction zones release ~90% of the total global seismic moment, and thus constitute much of the Earth's seismic potential. To better determine the seismic potential of a specific subduction zone, the spatial and temporal distribution of elastic strain accumulation and release along the plate boundary underthrust must be understood. The simplest description of subduction thrusts involves an interseismically locked depth interval (from 5–10 km to 30–70 km in depth) of the plate boundary interface that is bounded both updip and downdip by portions of the fault zone that deform aseismically (Figure 1) [*Savage*, 1983]. The width of the seismogenic zone, measured perpendicular to strike, varies widely both along and between the world's subduction zones [*Pacheco et al.*, 1993; *Tichelaar and Ruff*, 1993; *Oleskevich et al.*, 1999].

[3] Comparisons of plate motions and estimated locking widths with observed seismic moment release indicate that large portions of the subduction interface may slip aseismically [*Pacheco et al.*, 1993; *Tichelaar and Ruff*, 1993; *Wang and Dixon*, 2004]. Initially, estimates of the width of the seismogenic zone and its degree of kinematic coupling came from seismic records of earthquake occurrence and historic moment release [*Pacheco et al.*, 1993; *Tichelaar and Ruff*, 1993]. Geodetic measurements of surface velocities allow for direct estimation of the pattern of nonslipping and creeping fault segments during the period of geodetic observations (Figure 1b). GPS measurements of recent interseismic deformation along subduction zones throughout the world reveal that some plate interface faults are for the most part locked [*Mazzotti et al.*, 2000], others appear only partially locked [*Lundgren et al.*, 1999], while some appear to be accommodating convergence by steady aseismic slip only [*Freymueller and Beavan*, 1999].

[4] The occurrence of aseismic slip can vary with time, and thus inferences about kinematic coupling from geodetic data spanning a few years do not necessarily predict the degree of eventual seismic coupling evidenced in the distribution of seismic moment release. Even a subduction zone that appears completely nonslipping for long periods

[1]Department of Earth and Planetary Science, University of California, Berkeley, California, USA.
[2]Lamont-Doherty Earth Observatory, Palisades, New York, USA.
[3]Russian GPS Data Acquisition and Analysis Center, Geophysical Service of Russian Academy of Sciences, Moscow, Russia.
[4]Now at Department of Geological and Environmental Sciences, Stanford University, Stanford, California, USA.
[5]KOMSP, Geophysical Service of Russian Academy of Sciences, Petropavlovsk, Russia.

0148-0227/05/2005JB003648$09.00

of time might accommodate significant amounts of aseismic fault slip by postseismic afterslip [*Heki et al.*, 1997; *Mazzotti et al.*, 2000; *Bürgmann et al.*, 2001; *Miyazaki et al.*, 2004] or transient slow slip events [*Hirose et al.*, 1999; *Dragert et al.*, 2001; *Miller et al.*, 2002]. *Heki et al.* [1997] used continuous GPS measurements to show that rapid deformation over the first year following the 1994 Sanriku subduction earthquake in northeastern Japan was due to continued aseismic slip, which occurred mostly downdip of the coseismic rupture [*Yagi et al.*, 2003]. This slow slip event released a greater moment (4.2×10^{20} Nm) than the earthquake itself (3.1×10^{20} Nm, corresponding to M_w = 7.6). *Hirose et al.* [1999] document afterslip following two moderate subduction earthquakes in southwestern Japan, which were followed a few months later by a separate slow slip event of comparable moment about 200 km north of the epicenters. *Miyazaki et al.* [2004] invert 30 days of GPS data collected following the 2003 Tokachi-oki earthquake to find afterslip equivalent to an M_w = 7.7, which apparently occurred on velocity-strengthening portions of the plate interface adjacent to the coseismic rupture. *Bürgmann et al.* [2001] investigate a phase of rapid aseismic afterslip during two months following the 5 December, 1997 Kronotsky earthquake along the Kamchatka subduction zone. Rapidly decaying fault slip near the downdip edge of the coseismic rupture aseismically released as much moment as the M_w = 7.8 earthquake.

[5] A number of factors have been suggested that control the extent of the seismogenic portion of the subduction thrust, which may vary in space and time. The updip aseismic zone has been related to material properties in the shallow, unconsolidated accretionary prism that contains stable-sliding clay minerals. The transition in behavior of clay minerals appears to be sensitive to temperature [*Oleskevich et al.*, 1999], and thus the upper aseismic zone is predicted to be wider for older and colder downgoing oceanic crust. The downdip transition to aseismic deformation also appears to be temperature controlled, indicating a transition to aseismic slip at ~350°C and ultimately to viscous flow at higher temperatures that allow for crystal-plastic flow of rocks in the subduction zone. However, the lower transition might also be related to the juxtaposition of the plate interface with stable-sliding hydrated mantle material of the forearc. *Oleskevich et al.* [1999] suggest that the lower transition depth is defined by the 350°C isotherm or the crustal thickness of the overriding plate, whichever comes first; however exceptions to this pattern have been noted [*Simoes et al.*, 2004]. In addition to temperature-related phenomena, the plate convergence rate and/or the absolute velocity of the upper plate, the size and composition of the accretionary wedge, and the existence of heterogeneous features (such as seamounts) on the downgoing plate may lead to differences in effective stresses, temperature, permeability, and fault morphology that may favor seismic stick slip or stable aseismic slip. Recently *Wells et al.* [2003] and *Song and Simons* [2003] proposed a general global correlation of negative free-air gravity anomaly regions and associated topographic basins along subduction zones with the major subduction asperities that break in great earthquakes. While *Wells et al.* [2003] suggest the source of this relationship to lie in the possible role of subduction erosion, *Song and Simons* [2003] suggest that the forearc structure is indicative of variations in frictional properties and shear stress on the plate interface. Both consider the possibility that variations in slip behavior may act to cause the forearc anomalies they observe. Alternatively, the mechanical and structural properties may be consequences of other external factors mentioned above.

[6] Comparison of the source areas of large historic subduction earthquakes and nonslipping fault areas deduced from geodetic data suggests that asperities on the subduction interface are persistently locked interseismically, slip in large stick-slip events and are surrounded by areas of stable sliding. Thus the subduction thrust system appears to be a spatially heterogeneous system [*Pacheco et al.*, 1993; *Yamanaka and Kikuchi*, 2004] that may potentially evolve over time. This kinematic view of fault asperities makes no inferences about the frictional strength of either the nonslipping or creeping patches of the fault [*Lay and Kanamori*, 1981], but asserts their existence on the basis of direct observations. In this paper, we hypothesize that the Kamchatka subduction zone is a heterogeneously locked thrust fault dominated by persistent asperities that have failed in the past and will do so again in the future. Given the ~80 mm/yr plate convergence rate, we expect that most asperities have failed during the >200-year period of historic observations. However, as the occurrence of the 26 December 2004, $M \approx 9$ Sumatra-Andaman earthquake dramatically illustrated, this expectation may well be questionable. To test this hypothesis, we compare the results of distributed slip inversions formally derived from recently collected geodetic data with forward models in which we specify locked asperities defined by large historic rupture zones and solve for slip on the remaining fault surface utilizing zero-stress boundary conditions on those areas of the fault that slip freely around the locked portions of the interface. Using different asperity distributions, we test the consistency between inferred areas of locking along the subduction interface and past rupture distributions. In this way, we test the idea that asperities are long-lived features that persist over several earthquake cycle and may be defined on the basis of large historic ruptures.

2. Kamchatka Subduction Zone

2.1. Regional Tectonics

[7] The Kamchatka subduction zone accommodates underthrusting of the Pacific plate beneath the North American plate, or beneath a smaller microplate called the Okhotsk plate that is thought to include portions of eastern Siberia, the Okhotsk Sea and Kamchatka [*Seno et al.*, 1996; *Steblov et al.*, 2003]. The Pacific plate subducts at ~80 mm/yr, increasing from 77 mm/yr oriented toward 308° at 55°N to 83 mm/yr toward 301° at 47°N [*DeMets et al.*, 1990; *Steblov et al.*, 2003]. The Kamchatka subduction zone intersects the Aleutian trench near 55°N, but shallow distributed seismicity continues northward for about ~300 km (Figure 2). Plate convergence is nearly perpendicular to the ~35° strike of the Kamchatka subduction zone, and active deformation within the arc appears to be relatively minor [*Tibaldi*, 2004].

[8] The Pacific–North America plate motion is subparallel to the strike of the westernmost Aleutian arc, which

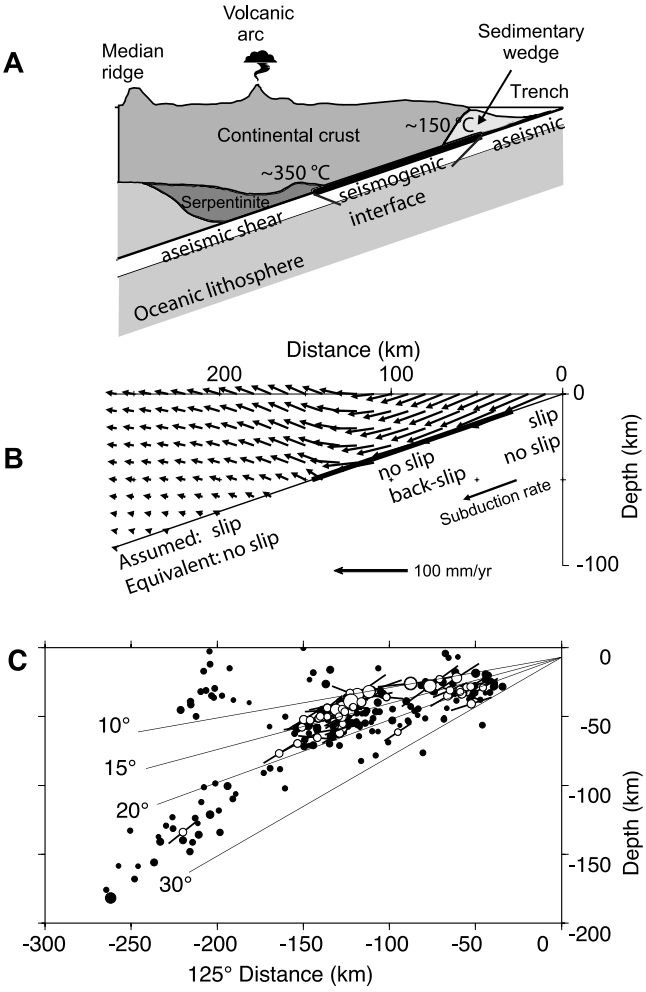

Figure 1. (a) Schematic cross section of the first-order geometry and factors of subduction zone locking of the Kamchatka subduction zone. (b) Dislocation solution for velocities within the overhanging wall relative to the plate interior. Identical deformation fields result from the assumed (slip on plate interface adjacent to locked portion) and equivalent back slip model scenarios. Variations in the locking width and degree of kinematic coupling result in changes in the predicted surface velocity field. Thus inversions of surface GPS velocities can be used to invert for the optimal subsurface locking pattern across and along a subduction zone. (c) Example of seismicity cross section used to establish the geometry of the subduction system. The data in the plot are projected from a 100-km-wide section oriented N125E and centered about a point at 52.5°N, 161.5°E. Solid circles are relocated hypocenters from the catalog of *Engdahl et al.* [1998]. Open circles are thrust events with lines indicating the dip of the west dipping nodal plane of Harvard centroid moment tensor (CMT) thrust focal mechanisms projected into the line of section. The CMT mechanisms are plotted at their respective Engdahl catalog hypocenter location, as the CMT catalog locations appear systematically eastward shifted by about 40 km. The lines indicate 10°, 15°, 20°, and 30° dipping dislocation planes emanating from the trench at 7 km depth.

thus forms a transform boundary intersecting and terminating Kamchatka subduction. Current deformation along the western Aleutians apparently occurs along a broadly distributed zone of strike-slip faulting [*Geist and Scholl*, 1994]. Focal mechanisms indicate strike-slip motion both north and south of the Komandorsky Islands, including Bering Island (Figure 2). This broad zone of shear deformation allows westward movement of the Aleutian Islands relative to stable North America, and so their accretion to the Kamchatka coast appears to be an important tectonic feature of this area. The subducting Pacific plate slab under Kamchatka terminates at the Kamchatka-Aleutian intersection [*Levin et al.*, 2002b]. In the mid-Cenozoic, subduction under northern Kamchatka appears to have occurred along the northwestern boundary of the Komandorsky basin in the Bering Sea, but ceased sometime since 10 Ma [*Geist and Scholl*, 1994; *Park et al.*, 2002].

2.2. Lithospheric Structure of Kamchatka and the Subducting Pacific Plate

[9] The kinematics and dynamics of a subduction zone can be related to the structure and nature of the hanging wall lithosphere. Crustal thickness estimates along the east coast of Kamchatka, determined from gravity measurements, active source seismic data [*Bogdanov and Khain*, 2000] and receiver function modeling [*Levin et al.*, 2002a], range from 30 to 40 km, comparable to the depth of the deepest plate interface thrust earthquakes. The uppermost mantle, below 40 km depth exhibits a convergence-parallel seismic anisotropy along the east coast of Kamchatka [*Levin et al.*, 2002a; *Park et al.*, 2002]. Shear wave splitting data suggest a trench-parallel mantle fabric below the subducting slab, which is terminated at the plate boundary corner [*Levin et al.*, 2002a; *Park et al.*, 2002].

[10] The kinematics of the plate interface may be related to the geometry and morphology of the subducting Pacific plate. The age of the downgoing Pacific plate increases from ~87 Ma in the north to ~105 Ma adjacent to the southern tip of Kamchatka which suggests a relatively uniform lithospheric thickness and buoyancy along the subduction zone. North of 54°N, the dip of the subducting slab at more than 80-km depths below Kamchatka shallows from 55° to 35° over a ~30-km distance and slab seismicity does not reach deeper than ~100 km [*Gorbatov et al.*, 1997]. This change in slab dip occurs below the seismogenic zone of the plate boundary thrust, but may still affect the shallow subduction process. Seismic imaging suggests that the lack of deep seismicity along the northern slab edge may be related to two possible Pacific slab delamination events during the last 5 m.y. These events can be linked to changes in island arc volcanism at ~5 Ma (cessation of arc volcanism in northern Kamchatka) and ~2 Ma (enhanced volcanism at Klyuchevskoi, the highest active volcano in Eurasia) [*Levin et al.*, 2002b; *Park et al.*, 2002]. A major change in morphology of the subducting Pacific plate occurs at 53.5–54.5°N, where the Meiji seamounts, which are the northernmost extension of the Hawaii-Emperor seamount chain, approach the subduction zone. *Gorbatov et al.* [1997] suggest that the density variations of the hot spot influenced lithosphere caused the nearby change in subduction slab dip angle and seismicity. Subduction of the Kruzenstern fracture zone

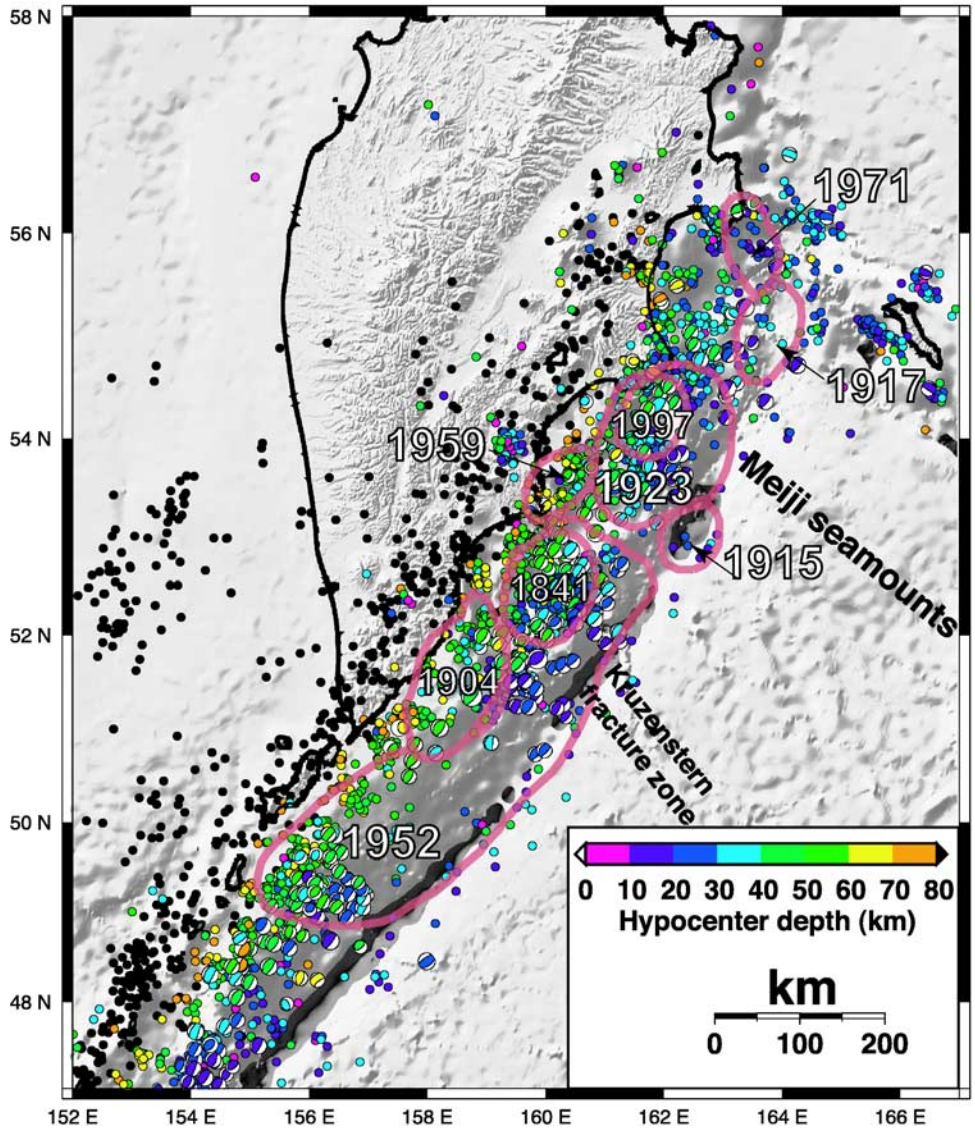

Figure 2. Instrumentally recorded seismicity and historic rupture zones of Kamchatka. Epicenters are from the most recent update (available at http://earthquake.usgs.gov/scitech/centennial/) of the relocated catalog of *Engdahl et al.* [1998] with a color scale indicating the source depths of the events down to 80 km depth. Black circles are in-slab events deeper than 80 km. Focal mechanisms are for 1977–2004 events at $\leq$80 km depth from the Harvard CMT catalog. Thrust mechanisms are color-coded according to the same depth scale. Bold red outlines labeled with year are the rupture zones of large historic earthquakes determined from aftershock distributions [*Johnson and Satake*, 1999].

near 52.5°N also appears to perturb the seismicity patterns and forearc structure.

2.3. Historic Seismicity

[11] The distribution and geometry of historic subduction earthquakes provide complementary information about the geometry and degree of seismic coupling of the plate interface. Several major earthquakes occurred during historically reported times, including $M > 8$ ruptures in 1904 (M_s = 8.0), 1923 (M_w = 8.5), 1952 (M_w = 9.0), and 1959 (M_w = 8.2), and the M_w = 7.8 1997 Kronotsky earthquake (Figure 2). The 4 November 1952 great Kamchatka earthquake was the fourth-largest earthquake of the 20th century, which generated Pacific-wide tsunamis and ruptured a 600- to 700-km-long and ~100-km-wide segment of the subduction interface. A great earthquake in 1737 is thought to have been a possible prior 1952-type event, suggesting a ~200-year repeat interval [*Johnson and Satake*, 1999]. *Johnson and Satake* [1999] use tsunami waveforms recorded throughout the northwest Pacific to infer that only the deeper portion (below ~20 km depth and assumed to dip 13°) of the plate interface experienced significant coseismic slip, which was localized on three major rupture patches with offsets of 6–12 m. This suggests that the shallower portion of the subduction thrust either slips aseismically or experiences separate outer rise ruptures that make up the slip differential. Large aftershocks were relatively sparse in the areas of high slip. Six $M \sim 7$ 20th

century earthquakes (three in 1904, one in 1973 and two in 1993) occurred near the southern high-slip segment of the 1952 event, while the 1959 $M_w = 8.2$ event initiated close to the northern 1952 slip maximum. Another great earthquake in 1923 apparently ruptured the subduction interface immediately north of the 1952 and 1959 rupture segments [*Johnson and Satake*, 1999]. Two $M_s > 7.5$ events in 1969 and 1971 located within and just south of the complex Kamchatka-Aleutian juncture, respectively, had shallow, west dipping nodal planes [*Geist and Scholl*, 1994].

[12] The 5 December 1997 $M_w = 7.8$ Kronotsky earthquake occurred just north of the epicentral region of the 1923 event [*Fedotov et al.*, 1999; *Gordeev et al.*, 1999]. Analysis of teleseismic waveforms and the distribution of aftershock hypocenters reveal that the earthquake occurred on an ~24° northwest dipping fault plane at ~30 km depth and propagated from the hypocenter toward the southwest for ~90 km [*Sohn*, 1998; *Gordeev et al.*, 2001]. The Kronotsky earthquake was preceded by a swarm of foreshocks that commenced 49 hours before the main shock and included 34 $m_b > 4$ events just north of the hypocenter. *Gordeev et al.* [2001] interpret GPS time series for a few stations to suggest that the earthquake was also preceded by a large aseismic slip event. The largest foreshock ($M_w = 5.5$) occurred 3 hours prior to the main event and had a similar 22°NW dipping focal mechanism nodal plane. Aftershocks occurred over a ~200-km-long zone but were notably absent in the area of foreshock activity and the area of maximum slip further south [*Zobin and Levina*, 2001]. The average dip of the northwest dipping nodal planes of foreshocks and aftershocks [*Dziewonski et al.*, 1998] is 25 degrees. Postseismic afterslip over a 40-day period released about as much (aseismic) moment as the main shock [*Bürgmann et al.*, 2001] and appeared to extend across the region of foreshock seismicity.

[13] The ratio of the rate of slip estimated from moment release in large historic earthquakes to the total slip rate determined from plate motion models provides an estimate of seismic coupling averaged over decades or centuries [e.g., *Pacheco et al.*, 1993]. The Kamchatka subduction zone appears fully coupled across a ~100-km-wide zone south of 53°N (dominantly breaking in 1952-type earthquakes), and only 40–50% coupled along the northern arc [*Pacheco et al.*, 1993]. *Pacheco et al.* [1993] report a locked-to-creeping transition depth of 55 km bounding a 97-km-wide seismogenic zone. *Tichelaar and Ruff* [1993] determine depths of five moderate earthquakes thought to be located at the downdip edge of the 1952 rupture to suggest a locked seismic interface in southern Kamchatka extending to 38–40 km depth with a dip of 28° at that depth.

2.4. Geometry of the Plate Interface

[14] The depth distribution of earthquakes along the Kamchatka subduction zone and nodal plane dips of moderate to large earthquakes help define the geometry of the subduction interface (Figure 1c). While the top of the slab seismicity and slab dip below ~80 km are well defined, the seismicity at shallower depth is diffuse and event depths are not well constrained [*Gorbatov et al.*, 1997]. The downdip limit of thrust focal mechanisms lies at about 60 km depth and roughly follows the coastline above [*Gorbatov et al.*, 1997; *Wells et al.*, 2003]. We use a relocated catalog of teleseismic earthquakes [*Engdahl et al.*, 1998] in the region to constrain the geometry of the subduction thrust. We trace the top of the slab seismicity along cross sections spaced 100 km up to 60 km depth and along the presumed plate interface to the ~7-km-deep trench to determine the average dip of the seismogenic plate interface. As there is significant seismicity both in the hanging wall and in the downgoing Pacific lithosphere, the geometry of the shallow plate interface is not well resolved. We find an average fault dip of 15° for the seismogenic portion of the plate boundary fault, with the actual fault dip probably increasing from ~10° near the trench to about 25° at ~60 km depth (Figure 1c).

[15] If large events occur dominantly on the plate interface, focal mechanism solutions should provide additional constraints on the subduction thrust dip. The 1977–2004 Harvard-CMT-catalog locations appear systematically eastward shifted by about 40 km with respect to the Engdahl catalog hypocenter locations (Figure 2). As this shift is independent of the event type involved and several thrust events are mapped to locations seaward of the trench, we suspect that this is a systematic mislocation, rather than being indicative of a real systematic hypocenter-moment centroid offset. Thus, when utilizing the CMT events, we use their Engdahl catalog hypocenter locations in the cross sections we construct (Figure 1c). Overall, the shallow nodal planes of the northeast striking, thrust-fault focal mechanisms appear to dip steeper than our favored 15° average thrust dip. This suggests that some of these events are not plate interface earthquakes, but occurred on thrust splays in the accretionary wedge and/or in the downgoing Pacific plate [*Okada et al.*, 2004].

3. GPS Measurements of Interseismic Surface Velocities

[16] Our data set consists of continuous (CGPS) and survey mode GPS (SGPS) measurements on and near Kamchatka (Figure 3). The five CGPS sites in the study region have been operating for more than 4 years [*Steblov et al.*, 2003]. Annually repeated observations at the 18 SGPS sites we consider were carried out in 2001, 2002 and 2003 using Ashtech Z-12 GPS receivers with choke ring antennas at all stations. Each site was observed in 24-hour sessions for 4–5 days, to get redundant data and to suppress short-period, day-to-day noise. Observations at each primary site were accompanied by simultaneous observations at two to three offset sites in the immediate neighborhood, to allow for characterization of the local stability of the main mark by comparison with the reference points.

[17] The data were analyzed as described by *Steblov et al.* [2003]. We use the GAMIT software [*King and Bock*, 2002] to process the GPS phase observations from the regional network that includes the Kamchatka sites together with six to seven International GPS Service (IGS) stations. We then used the GLOBK Kalman filter [*Herring*, 2002] to combine station coordinates and their covariances with similar solutions for the global IGS network available from the Scripps Orbital and Permanent Array Center (SOPAC). Combination of these quasi-observations yields a single solution for positions and velocities over the full span of

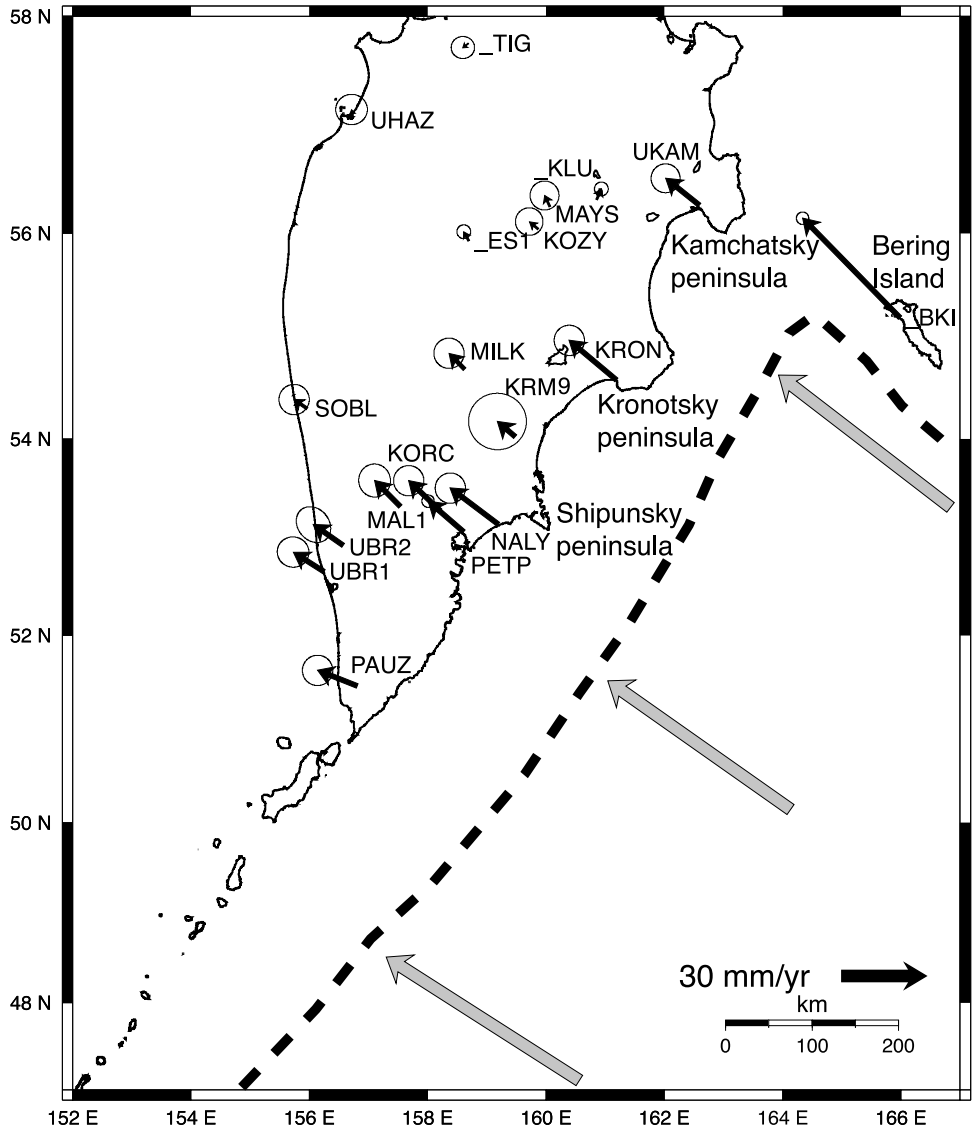

Figure 3. GPS velocities in the Kamchatka region shown in a North American plate reference frame and tipped with 95% confidence ellipses. Offshore shaded arrows indicate Pacific plate velocities at the trench computed from the plate rotation parameters that were derived from the GPS velocities of sites located within the plate interior.

the data. We adopted an error model for the observations that reflects both the scatter in the (∼monthly) estimates of position and the effect of temporal correlations. We add 2 mm random and 2 mm/(yr)$^{1/2}$ random walk noise to the uncertainty of horizontal position of all stations within each solution.

[18] At each step of the processing, we impose only loose constraints on the station coordinates so that the reference frame can be defined later. To map the loosely constrained multiyear solution to constrained station velocities, we introduce reference frame constraints by setting a priori velocities for a subset of plate interior stations. We follow *Steblov et al.* [2003] to define a three-plate GPS reference frame including 38 stations; their velocities were minimized on North America (14 stations), and constrained to values predicted with GPS-estimated rotation vectors in Eurasia (18 stations) and on the Pacific plate (6 stations). The velocity field used in the inversions is in the North American reference frame (Figure 3 and Table 1).

4. Models of Interseismic Slip Along the Kamchatka Subduction Zone

[19] Horizontal GPS station velocities and their uncertainties allow us to develop first-order models of the deformation using elastic dislocation models and model optimization methods. In our model inversions we utilize the standard model of a back slipping rupture interface [*Savage*, 1983]. In this idealization of interseismic strain, surface deformation is assumed to be produced by aseismic slip downdip and updip of a (partly) locked zone. Assuming that the Earth deforms as a linear elastic half-space, deformation from this scenario is equivalent to the sum of the deformation expected from backward slip on the locked

Table 1. GPS Velocities

Longitude, °E	Latitude, °N	E-Velocity, mm/yr	N-Velocity, mm/yr	σ_E, mm/yr	σ_N, mm/yr	E-N Velocity Correlation	Station
212.501	64.978	0.5	−1.2	0.8	0.7	0.000	FAIR
166.438	68.076	0.9	−0.7	0.8	0.8	0.000	BILI
166.211	62.456	0.4	2.1	0.8	0.8	0.001	_KMS
166.147	60.445	−4.6	−5.9	1.1	1.1	−0.003	_TIL
165.984	55.192	−34.6	35.4	0.9	0.9	0.000	_BKI
163.067	59.243	0.1	1.6	2.2	2.2	−0.001	OSSO
162.593	56.265	−12.0	9.6	2.1	2.1	0.002	UKAM
161.194	54.585	−16.8	14.1	2.2	2.2	−0.002	KRON
160.856	56.318	1.7	3.8	1.0	1.0	0.000	_KLU
160.062	56.254	−1.8	3.9	2.1	2.1	0.001	MAYS
159.865	56.042	−3.1	2.6	2.0	2.0	0.000	KOZY
159.481	54.025	−6.3	5.4	4.2	4.1	−0.006	KRM9
159.197	53.142	−17.1	12.9	2.2	2.2	0.000	NALY
158.697	55.930	−1.8	3.2	1.0	1.0	0.000	_ES1
158.686	57.759	−1.9	−1.5	1.7	1.6	0.001	_TIG
158.623	54.693	−5.5	5.6	2.2	2.2	−0.003	MILK
158.607	53.067	−12.6	10.9	0.9	0.9	0.000	PETP
158.213	53.280	−11.2	10.7	2.2	2.2	0.001	KORC
157.536	53.325	−9.1	9.2	2.3	2.4	−0.011	MAL1
156.810	51.466	−14.1	5.6	2.2	2.2	0.004	PAUZ
156.738	57.091	−0.5	2.5	2.3	2.2	0.002	UHAZ
156.575	52.928	−10.6	7.4	2.5	2.6	−0.206	UBR2
156.244	52.661	−10.9	6.9	2.3	2.2	−0.016	UBR1
155.962	54.304	−4.6	3.2	2.2	2.2	0.000	SOBL
155.770	62.518	−0.3	0.8	2.3	2.2	−0.003	OMS1
152.392	61.130	1.4	−2.6	2.3	2.2	−0.001	TAL1
152.422	62.925	−0.6	−0.6	1.2	1.2	0.001	SEY2
150.770	59.576	−1.4	−2.1	1.0	1.0	0.000	MAG0
148.168	62.779	0.4	−1.0	1.2	1.2	0.000	SUS1
147.431	61.883	1.8	−3.8	1.3	1.3	−0.001	KUL1

fault sections and rigid block translation at long-term rates across the full plate boundary interface (Figure 1b) [*Savage*, 1983]. Thus the magnitude of the back slip rate relative to the long-term subduction rate provides an estimate of the degree of kinematic coupling across the plate interface. A back slip rate equaling the plate convergence rate corresponds to a nonslipping fault patch, while a zero back slip rate indicates free slip. We assume that all strain that accumulates interseismically is elastic and is recovered during later times in the seismic cycle, which assumes the geodetically measured deformation field is not contaminated by contributions from permanent geologic strains. In the inversions we employ rectangular [*Okada*, 1985] and triangular [*Thomas*, 1993], uniform-slip dislocations embedded in an elastic, homogeneous and isotropic half-space. Table 2 summarizes the geometry parameters, slip rate and misfit statistics of the models we present below.

[20] In addition to the kinematic back slip inversions, we investigate models in which the aseismic portion of the plate interface is parameterized with stress boundary conditions loaded by back slipping (i.e., locked) sections of the fault plane and superposing the regional plate convergence rate. This approach allows us to explore if locked asperities that are defined by the rupture areas of major historic earthquakes and are surrounded by aseismically slipping portions of the subduction interface can produce the geodetic velocities.

4.1. Optimal Fault Geometry From Nonlinear GPS Inversions

[21] To estimate the geometry of the interseismically locked fault directly from the geodetic data, we use a constrained, nonlinear optimization algorithm [*Bürgmann et al.*, 1997]. The inversion solves for the best fit rectangular

Table 2. Summary Information on Geometry Inversions

Model	Length, km	Width, km	Dip, °NW	Strike, °	Center Latitude, °N	Center Longitude, °E	Locking Depth, km	Slip Rate, mm/yr	Sigma, mm/yr	WRSS, mm^2/yr^2
1	934	163	10	35	51.95	161.35	32.6	53	2	89.8
2	640	125	21	35	51.95	161.35	50.1	80[a]		90.2
3a	406	222	12	35	50.57	159.50	49.6	46	3	58.5
3b	480	108	12	35	54.05[a]	162.80[a]	26.8	54	4	58.5
4a	457	163	15	33	50.27	159.80	45.9	80[a]		69.5
4b	469	80	15	35	54.05[a]	162.80[a]	25.1	80[a]		69.5
5a	300[a]	189	28	35	50.93	160.10	94.3	80[a]		52.0
5b	475	93	7	34	54.05[a]	162.80[a]	16.3	80[a]		52.0

[a]Value is constrained or reaches a bounding value.

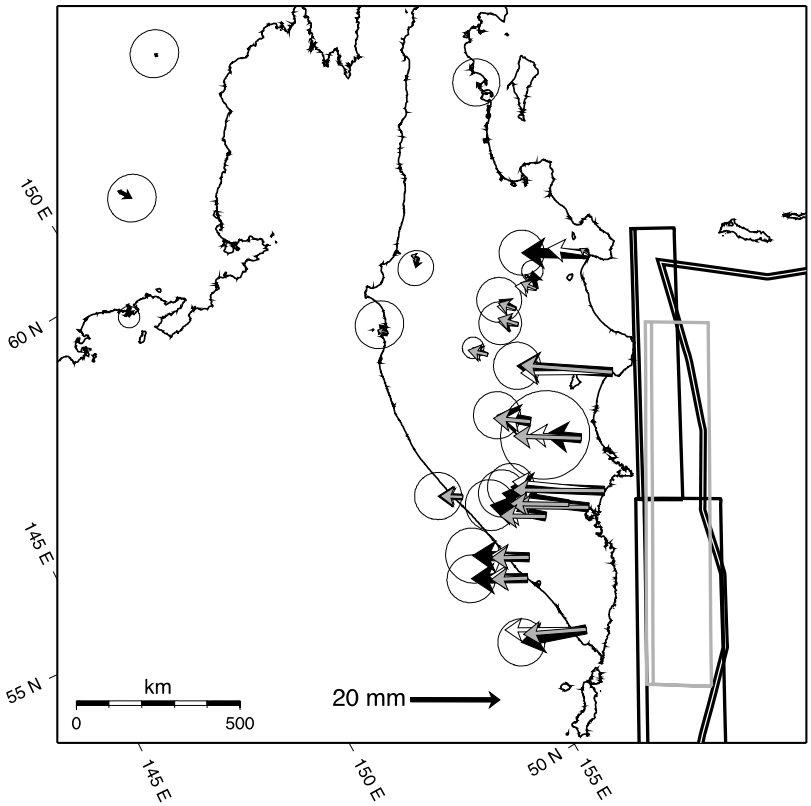

Figure 4. Optimal one- and two-dislocation back slip models inverted from the horizontal GPS velocities (solid arrows tipped by 95% confidence ellipses) shown relative to North America. Map is in an oblique Mercator projection about the angular rotation pole of North America–Pacific motion computed by *Steblov et al.* [2003]. Thus convergence-parallel features or velocities are aligned with the map border. The shaded (single-fault) and solid (two-fault) dislocation planes represent fully locked portions of the subduction thrust leading to the predicted velocity field. Modeled velocities are shown as shaded and open arrows for the one-fault and two-fault models, respectively. Even this simple model allows us to conclude that the degree of coupling and inferred locking width significantly decreases from south to north.

dislocation geometry (parameterized by length, depth, width, dip, strike, and location) and the fault slip rate. The optimization routine seeks to minimize the weighted residual sum of squares $WRSS = (d - m)^{\mathrm{T}} cov^{-1} (d - m)$, where d and m are the GPS observed and modeled horizontal motions, respectively, and cov is the data covariance matrix that accounts for correlations between the east and north velocity components of all stations. We consider models in which we allow one or two back slipping fault surfaces and explore the effect of solving for the geometry when both are fully locked (back slipping at the full plate convergence rate of 80 mm/yr), and when each is allowed to have different back slip values that are treated as free parameters in the inversions (Table 2).

[22] The upper edge of the locked fault plane is defined by the bathymetric expression of the 7-km-deep subduction trench. We apply bounds on the strike (N33–35°E) and rake (dip slip only) of the dislocation(s) in the inversion. Thus we focus on resolving only the along-trench extent, the downdip width and the dip of the locked plate interface. Assuming a completely locked, single asperity along the Kamchatka subduction zone (i.e., back slipping at the full plate convergence rate of 80 mm/yr), we find an optimal width of 125 km of a 21°NW dipping fault plane reaching down to 50 km depth (Figure 4). The WRSS of this model is 90.2. The northern tip of the 640-km-long dislocation plane lies well south of the Aleutian arc. If we add the back slip rate to the list of estimated parameters, the optimal dip and width of the asperity are, 10° and 163 km, respectively, with a back slip rate of 53 mm/yr, resulting in a comparable WRSS of 89.8. The locking depth implied by this more shallowly dipping model is 33 km. However, single-dislocation models produce systematic misfits to the observed velocities in that the modeled inland velocities are too low in southern Kamchatka, suggesting a greater degree of kinematic coupling along that portion of the subduction zone.

[23] Next, we consider two-segment models, in which we solve for the geometry and dip of two adjoining dislocation planes. All two-dislocation models favor a wider and more deeply locked back slip plane to the south (Table 2 and Figure 4). If we allow for differences in dip between the two planes, the model favors significantly steeper dips in the south (28° versus 7°) resulting in a 94 km locking depth for the southern segment. If we solve for a common dip of the two back slip planes, the optimized dip is 15° for a fully

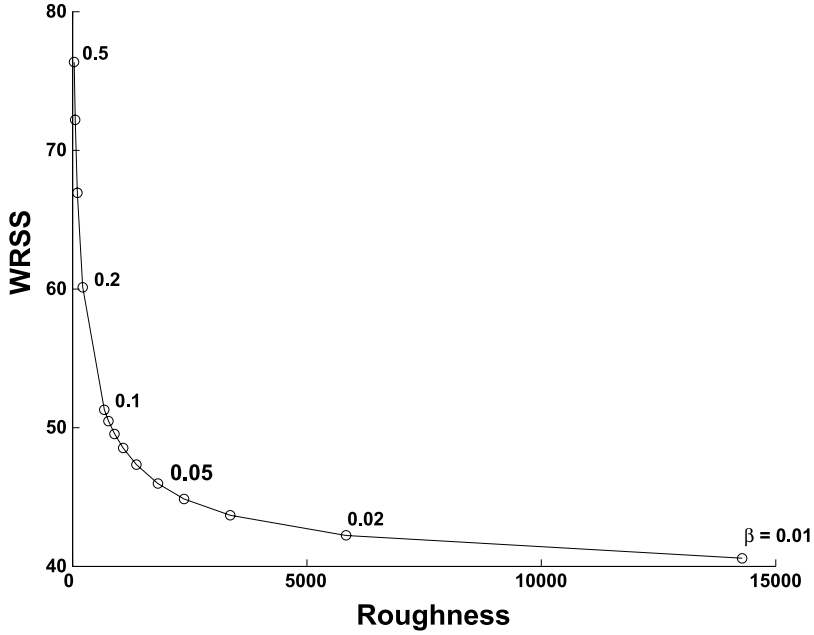

Figure 5. Tradeoff curve between model roughness and misfit (WRSS) of the distributed slip model velocities to the GPS data, depending on the weight (β) put on smoothing in the inversion.

locked, and 12° for a partly locked interface. The WRSS of the two-fault models vary between 52 and 70, depending on the choice of parameter constraints (Table 2). The models favor a more narrow, and possibly more shallowly dipping, nonslipping interface north of ~52° latitude. Remaining significant misfits suggest that these first-order models that require constant back slip along large portions of the fault plane may not capture the full complexity of the locking pattern revealed by the data. The geodetic data alone do not uniquely constrain the geometry of the locked subduction interface; therefore we incorporate additional constraints from the seismicity when parameterizing the subduction interface in the distributed slip models described below.

4.2. Distributed Slip Models

[24] While the two-patch dislocation models provide a broad-scale picture of how slip may be accommodated along the subduction interface, finer details of the slip distribution may be inferred from the geodetic data by first defining the fault geometry from bathymetry and microseismicity, and then using two alternative approaches: (1) Solve for the slip distribution that best describes the observed surface velocities and (2) determine the slip distribution and surface velocities resulting from loading of locked asperities defined by historic earthquake ruptures.

[25] Our model geometry is based on the observed seismicity along the subduction zone. The plate interface is divided into five segments, which dip 15° toward the Peninsula; however, the strike of the segments varies from 42° in the south to 14° in the north. The modeled subduction interface extends to a depth of 60 km, below which continuous aseismic slip is assumed to accommodate plate convergence. These planar segments were discretized into 2,153 triangular elements.

[26] A well established 3D BEM code, Poly3D [*Thomas*, 1993] is used for this work. Poly3D divides the fault plane into triangular elements, so that complicated three-dimensional fault geometries are easily pursued. Poly3D allows both displacement and traction boundary conditions to be imposed on fault surfaces and calculates the resulting stresses and deformation within a linear elastic half-space. These different boundary conditions may be imposed for different modes of displacement and traction; for example, we can prohibit opening or closing along the fault plane, but allow a specified shear stress drop along the element surfaces, resulting in strike-slip and/or dip-slip displacement discontinuities. In the distributed slip inversions, we only allow slip to occur in the direction of plate convergence (307°) and prohibit opening along the fault plane. In the boundary element asperity models, we allow full shear stress drop along those elements of the subduction interface that slip aseismically and specify a displacement discontinuity on the locked asperity patches. By differentiating the displacements with respect to time, we cast the surface and plate interface displacements in terms of surface velocity and slip rate boundary conditions, respectively.

4.2.1. Distributed Slip Inversions

[27] We invert for the optimal slip distribution and seek models that minimize the misfit (WRSS), while preserving some degree of smoothness of the model slip distribution. Smoothing and minimum and maximum slip rate constraints are applied to avoid models with unreasonable (oscillating) slip patterns that are favored by a free inversion without such additional constraints [*Harris and Segall*, 1987; *Du et al.*, 1992]. To avoid such oscillations, we minimize the curvature of the slip between elements [*Schmidt et al.*, 2005], similar to the finite difference approximation of the Laplacian that is commonly used to impose smoothness constraints on the slip distribution [*Harris and Segall*, 1987]. At the downdip edge of the modeled fault plane, we assume that the subduction interface accommodates the full plate convergence by steady

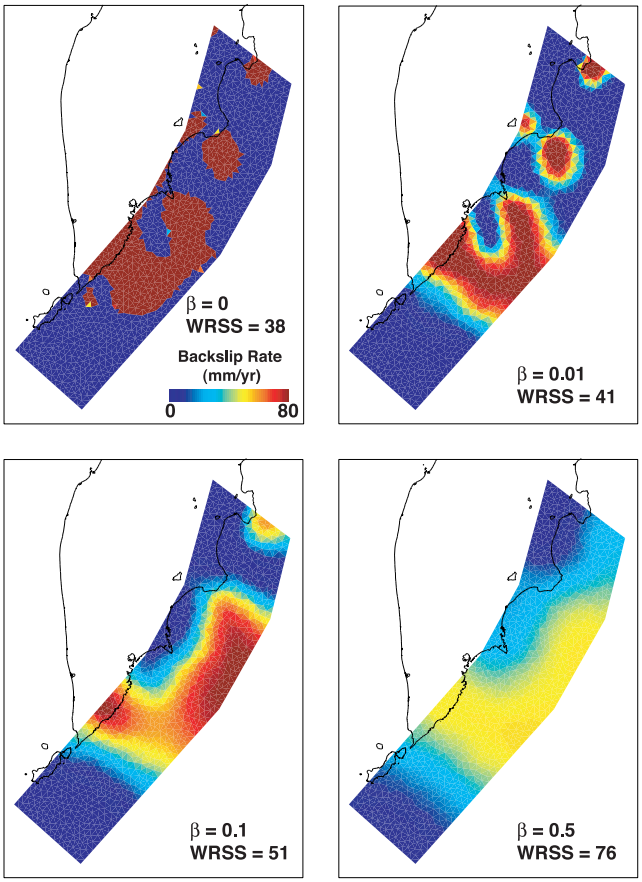

Figure 6. Distributed slip models on the 15°NW dipping dislocation plane discretized into triangular elements inverted from the horizontal GPS velocities using no smoothing (top left) and a range of smoothing weights considered in Figure 5. The smoothing includes a constraint to favor models decaying to zero back slip at the bottom edge of the model. The color scale indicates the coupling on the partially locked portion of the plate interface using the back slip approach of *Savage* [1983]. Back slip rates of 80 mm/yr indicate full locking, and rates of zero represent areas of aseismic slip at plate convergence rates. Slip rates outside of these two bounding values are not allowed.

slip, and so we impose a zero–back slip condition to the smoothing toward the bottom edge. We consider a wide range of weights on the smoothing constraints and choose a weighting factor (referred to as β in Figure 5) on the basis of visual inspection of the tradeoff between model roughness and misfit (Figure 5), and the resolution tests described below. We use the bounded variable least squares (BVLS) method [*Stark and Parker*, 1995] to impose the slip rate bounds [*Price and Bürgmann*, 2002]. Here, the back slip is constrained to range between 0 mm/yr, representing portions of the fault that slip freely at the plate convergence rate, and 80 mm/yr, representing areas that are inferred to be fully locked.

[28] Figure 6 shows the inverted slip distribution for a range of weights on the smoothing constraint. The models are also labeled with the respective WRSS misfits, which range from 38 for a model with no smoothing to 76 for a highly smoothed inversion. Figure 7a shows the slip model with a smoothing weight of $\beta = 0.05$ together with the observed and predicted GPS velocities. Independent of the degree of smoothing chosen, the models favor a nonslipping plate interface under southern Kamchatka, with the apparent locking reaching down to the lower edge of the back slip plane at 54 km depth. The inversion result for back slip on the plate interface north of ~53°N suggests significant aseismic slip below and between potentially locked patches. The current sparsity of GPS sites in southernmost Kamchatka and near the Aleutian-Kamchatka arc juncture limits our resolution in those areas. We plan to install additional sites in particular in the Aleutian-Kamchatka cusp region to better resolve the complex deformation that we expect to find at the northern termination of the subduction zone.

[29] We carried out resolution tests to ensure that the primary features in our model are well constrained by the data. We forward model surface velocities using a number of synthetic slip patterns (so-called checkerboard tests). In these simulations, we prescribe a regular, alternating grid to the fault plane using slip rates of 80 mm/yr and 0 mm/yr and calculate surface velocities at the GPS site locations, apply 0.3–3 mm/yr of noise to the velocities, weight the station velocities according to the observed velocity uncertainties, and finally reinvert for the optimal slip distribution using the approach described above. Figure 8 shows an example with a checkerboard patch size of approximately 60 by 200 km. The forward predicted velocities are inverted with a range of upper bounds on the back slip amplitude. Using the plate rate bound of 80 mm/yr we find that we can resolve the first-order slip pattern of the deeper fault elements under and just offshore Kamchatka, if noise applied to the forward modeled GPS velocities is $\leq$1 mm/yr. However, in the case that the noise in the GPS data is $\geq$3 mm/yr, we are unable to recover the first-order features of the checkerboard pattern. As expected, resolution decreases away from the GPS network toward the trench and in the south. The on-land GPS velocities are not able to resolve any detail of the back slip pattern far offshore along the trench. The addition of new GPS sites along the sparsely instrumented east coast of Kamchatka will improve the resolution of the offshore slip distribution. On the basis of a series of models with a range of slip patch sizes, we conclude that features of along-arc dimensions of 100–200 km are well resolved in the 20–50 km depth intervals of the plate interface.

4.2.2. Asperity Modeling

[30] The distributed slip inversion approach is purely kinematic, in that it solves for displacement discontinuities in the elastic half-space that optimize the fit to the surface GPS velocities. Alternately, Boundary Element Method (BEM) models [*Crouch and Starfield*, 1983; *Thomas*, 1993; *Bürgmann et al.*, 1994] allow for the parameterization of stress boundary conditions on fault elements thought to slip aseismically. Thus we can pursue models in which we impose loading and solve for slip on the plate interface with a heterogeneous strength distribution inferred from historic earthquake rupture asperities.

[31] A first-order example of this approach lies in the consideration of the <10-km-deep portion of the subduction zone that is commonly thought to be slipping aseismically. As GPS data on land rarely provide solid constraints on either the width or rate of slip on this portion of the fault, it

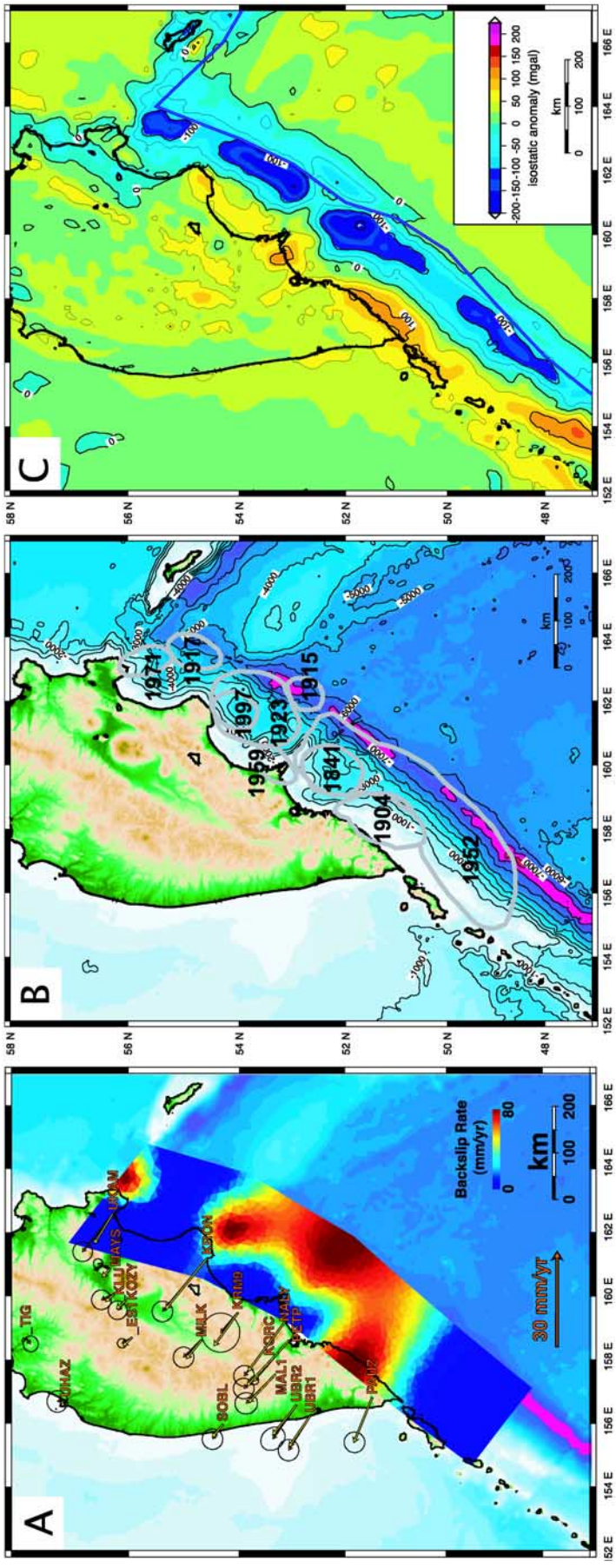

Figure 7. (a) Distributed slip model on modeled fault plane discretized into triangular elements and inverted from the horizontal GPS velocities using a smoothing factor $\beta = 0.05$. Observed (red arrows with 95% confidence ellipses) and modeled (yellow arrows) velocities are shown relative to a North American reference frame. The model indicates that the subduction zone is more coupled in the south, where the $M = 9$, 1952 earthquake and other major ruptures occurred. (b) Topography and bathymetry of the Kamchatka region shown with historic rupture zones from Figure 2. (c) Map of isostatic gravity anomalies over and offshore of Kamchatka. On-land data are from gravimeter measurements [*Kogan et al.*, 1994], and data over oceans are derived from satellite altimetry [*Sandwell and Smith*, 1997].

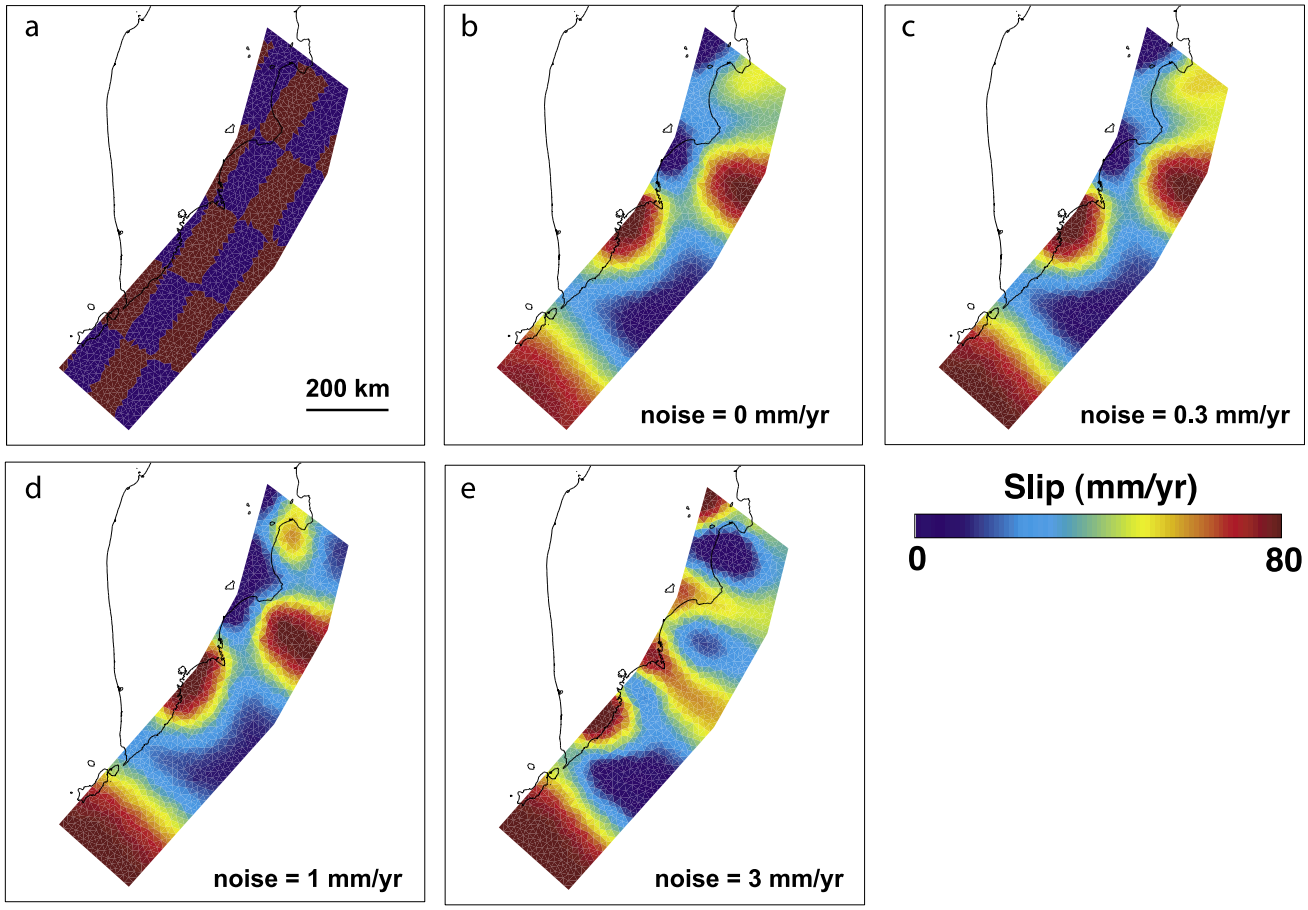

Figure 8. Resolution tests of GPS network geometry. (a) A regular, checkerboard pattern applied to the triangular mesh that defines the fault surface in the distributed slip inversions. Each patch was set to be 200 km and 60 km long in the along-strike and downdip directions, respectively. Minimum and maximum values of back slip were set to 0 (blue) and 80 mm/yr (red) to simulate freely slipping and fully locked portions of the fault plane, respectively. A smoothing factor of 0.05 was used which is the preferred value in the formal data inversions (Figure 7). (b–e) Fault slip distribution inverted from synthetic velocity data created using the checkerboard slip pattern. Randomly distributed noise of 0 mm/yr (Figure 8b), 0.3 mm/yr (Figure 8c), 1 mm/yr (Figure 8d), and 3 mm/yr (Figure 8e) was added to the synthetic velocities before inversion.

is often assumed to be slipping at a rate consistent with the long-term convergence rate [*Savage*, 1983]. However, even if the fault is creeping and very weak, stress shielding by the locked downdip fault surface will not allow it to achieve such a high slip rate [*Wang and Dixon*, 2004]. The BEM method allows us to develop models that produce more physically reasonable slip patterns that satisfy such constraints.

[32] We choose to load the fault plane by using a back slip approach similar to that used in the distributed slip models described above. Several alternative loading scenarios were considered in which deformation along the Kamchatka Peninsula was driven by prescribing velocities along the margins of the North American plate relative to the Pacific plate. In these scenarios, the base of the lithosphere was simulated as a surface on which a constant velocity discontinuity was prescribed, and aseismic portions of the dipping subduction interface were treated as shear traction-free surfaces with zero fault-normal displacement discontinuity. Locked asperities were simulated by requiring displacement discontinuities on the respective fault elements to be zero. The transition between the horizontal base of the lithosphere and dipping subduction interface produced elastic strain in the hanging wall of the subduction zone even in the absence of asperities. In contrast, the back slip approach assumes that all plate convergence is ultimately accommodated by slip on the subduction thrust [*Savage*, 1983].

[33] Asperities along the fault plane allow mechanical coupling between the Pacific and North American plates, and so these features act to apply downdip tractions to the Kamchatka lithosphere along the subduction interface. In this case, asperities may be simulated by applying a constant slip rate boundary condition along the inferred locked fault patches (slipping at plate rate of 80 mm/yr), allowing the adjacent areas of the fault plane to slip as a consequence of the loading imposed by this backward slip, and subtracting these displacement discontinuity rates from the relative plate convergence rate of 80 mm/yr.

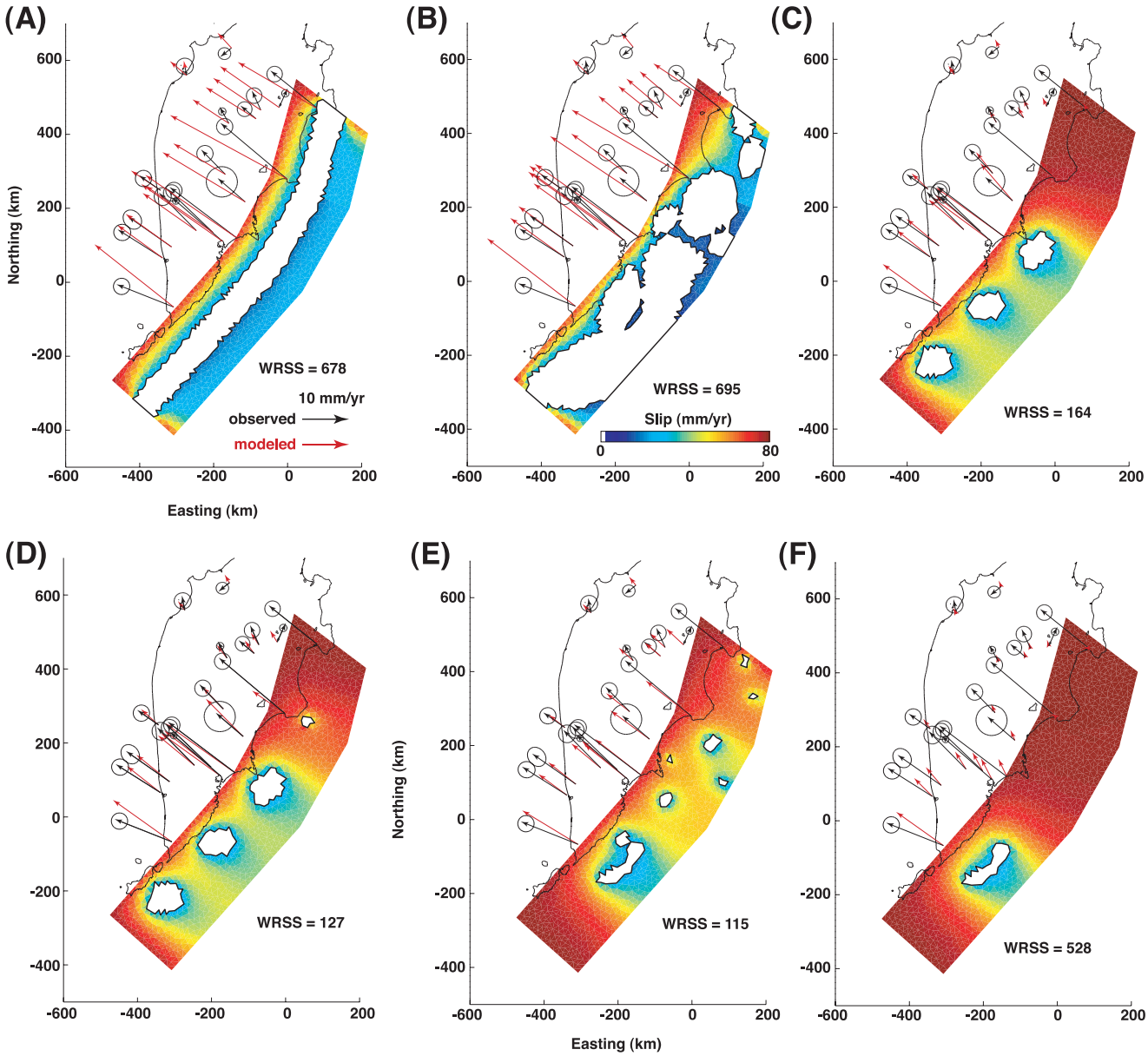

Figure 9. (a–f) Surface projection of the triangular dislocation mesh for use in the BEM modeling showing the five asperity scenarios considered. Shown in white are the zero-slip asperities. Colors of the triangular elements denote slip rate values calculated from forward models loading the fully locked rupture zones of historic earthquakes surrounded by a freely slipping (zero shear stress) plate interface exposed to plate convergence boundary conditions (see text for explanation). The observed and predicted station velocities are shown with solid black and red arrows, respectively.

[34] Normal-fault slip at plate convergence rate and azimuth is imposed along those elements that are considered to represent locked asperities along the fault plane. All other elements along the fault plane are allowed to slip so as to completely relieve the downdip and along-strike shear stress, while opening/closing is prohibited. Surface velocities are calculated at the locations of the GPS sites on the basis of this slip distribution, and the WRSS is calculated as in the slip inversions to assess the agreement between the measured and modeled surface velocities. Finally, the thrust slip distribution along the fault plane is recovered by subtracting the normal slip magnitude along each element from the plate convergence rate.

[35] We consider five different asperity distributions along the fault plane in our forward modeling (Figure 9). First, we assume a simple asperity distribution in which all elements between 20 and 40 km depth remained locked (Figure 9a). In this case, velocities are relatively uniform along the strike of the subduction zone, and decay monotonically away from it. A subtle rotation in velocity is observed in the vicinity of the along-strike bend in the subduction zone that causes the along-strike component of the velocities to be directed toward this bend. The stress shadow from the locked portion of the fault plane extends toward the surface, causing slip along the upper portion of the fault plane to remain low. The BEM overestimates the

measured velocities and produces a poor fit to the data (WRSS = 678).

[36] Next, we use the inferred extent of historic ruptures along the subduction interface (Figure 2) [*Johnson and Satake*, 1999] to create a locked asperity distribution (Figure 9b). This model assumes that all large earthquakes occur in the location of persistent asperities along the fault plane, while intervening portions slip aseismically. In addition, this model assumes that the full extent of historic ruptures, which was primarily estimated from the extent of aftershock zones, defines the locked portion of the fault plane. The dense, large asperities cause most of the areas of the fault plane to slip aseismically at rates significantly less than the plate convergence rate. The modeled velocities always overpredict the magnitude of the measured velocities, especially for sites in northern Kamchatka. This model fits the measured data slightly worse than the first geometry (WRSS = 695).

[37] The third asperity model explores a locking distribution that is defined by identifying portions of the 1952 rupture that experienced slip >6 m determined from inversion of tsunami data by *Johnson and Satake* [1999] (Figure 9c). This model postulates that only the high-slip portions of the largest earthquake ruptures constitute persistent asperities along the fault plane, while intervening portions may also slip aseismically. Hence this model results in less extensive kinematic coupling of the subduction interface than the other two geometries (Figure 9c). In this scenario, the stress shadow cast on the fault plane projects updip and reduces slip in those areas; however, the restricted size of the asperities allows higher slip rates updip of the asperities than the previous two models. Modeled surface velocities are higher in the south and decrease to the north as slip along the northern $\sim$1/4 of the modeled subduction zone returns to the plate convergence rate. The presence of locked asperities causes a clockwise rotation in the direction of the modeled velocities in the north relative to the south. This asperity model reproduces the observed northward decrease in velocity magnitudes and clockwise rotations (Figure 9c) and produces an improved fit to the data relative to the first two models (WRSS = 164). However, the BEM slightly underestimates the velocities of several sites located in the northern inland portions of Kamchatka, while greatly underestimating the rates of two sites along the coast in the north. Adding an asperity corresponding to the other well determined historic rupture, the 1997 Kronotsky earthquake to this asperity model produces a notable improvement in fit (WRSS = 127, Figure 9d).

[38] In our fifth model, we explore the possibility that long-lived asperities are nested at the location of former ruptures; however, the portion of the locked fault is far smaller than the entire inferred rupture extent. Noting that the high-slip areas of the 1952 rupture constituted approximately one quarter of the total rupture area [*Johnson and Satake*, 1999], we designed an asperity distribution by uniformly reducing each historic event to 25% of its inferred extent (Figure 9e). Because we have no information about how slip may have varied in space along each of the historic ruptures (excepting the 1952 event), we assume for simplicity that the high slip asperities for each rupture mimic the shape and lie in the center of the larger rupture. In this case, the absence of deep asperities results in slip close to the rate of plate convergence along the bottom $\sim$1/3 of the fault plane. The presence of smaller asperities along the northern half of the fault plane reduced slip in its shallow portions while deeper areas slipped freely. Velocities produced by this slip distribution generally decrease from south to north because of the reduced size and density of locked portions of the fault plane. The offshore asperities produce high velocities along the northern coast of Kamchatka, while allowing lower velocities within the interior portions of the Peninsula. When compared to the measured velocity distribution, this asperity scenario fit the data well, with much smaller misfit than the alternate scenarios we considered (WRSS = 115).

[39] In the last asperity scenario considered, we reduce the extent of the 1952 rupture to the central 25% of its rupture area (Figure 9f). This model was intended to gauge the importance of the details of the coseismic slip distribution on our definition of asperities. Tsunami data indicate that in the 1952 rupture, the high-slip portions of the fault plane were not confined to the center of the total rupture area but instead occurred in three discrete patches within the rupture (Figure 9c) [*Johnson and Satake*, 1999]. Surface velocities expected from this scenario underestimate the measured velocities in the northern portion of the Peninsula, where the fault plane slipped freely. Near the asperity, modeled velocities underestimate those observed, and a systematic south-to-north clockwise rotation in the velocity azimuths is observed (Figure 9f). This asperity scenario produces more than a threefold increase in the misfit between modeled and observed velocities relative to the high-slip asperity model considered in Figure 9c (WRSS = 528). Therefore the details of the slip distribution during the largest events may significantly impact the inferred asperity distribution.

5. Discussion

[40] Significant moment release by aseismic slip on the subduction thrust at depths $\leq$50 km helps explain the discrepancy between estimates of the seismic moment expected from plate convergence rates and the moment released in historic subduction zone earthquakes. The GPS velocity field measured on Kamchatka reveals first-order variations in the distribution of nonslipping and aseismically slipping portions of the plate interface along the Kamchatka subduction zone. The higher velocities with respect to the North American plate in southern Kamchatka suggest that a larger section of the fault is not slipping, or slipping at a reduced rate. In northern Kamchatka, kinematic coupling appears significantly reduced. This is consistent with the distribution of major historic earthquakes in the region.

5.1. Asperity Model of Subduction Zone Strain

[41] We find that a mechanical model of subduction zone strain that places small locked asperities in the core of historic earthquake rupture zones, and takes into account the stress shadowing from such locked zones during the interseismic period, appears to fit the GPS data well. Models in which we lock the full extent of historic rupture zones greatly overestimate the landward GPS velocities. If the ruptures did in fact extend as widely as assumed [*Johnson*

and Satake, 1999] this suggests that large regions surrounding the inner asperities are conditionally stable, that is, they are able to both slip aseismically at a reduced rate during the interseismic period and take part in a dynamic earthquake rupture [*Scholz*, 1998; *Lay and Schwartz*, 2004]. In regions of much reduced kinematic coupling and low historic seismic moment release, currently creeping portions of the subduction thrust appear to behave in a velocity strengthening fashion, accommodating all their offset via aseismic slip. Here aseismic slip is likely to accelerate because of increased loading following the neighboring asperity failures as documented in the aftermath of the 1997 Kronotsky earthquake [*Bürgmann et al.*, 2001].

[42] In addition to the major ($M_w > 7.5$) earthquake ruptures we considered in our asperity forward model, locked source areas of smaller events contribute to the degree of kinematic coupling of the subduction thrust. Individual contributions to the elastic strain field from smaller events are likely to be small, as the source dimensions of these earthquakes are much smaller [*Lutikov and Dontsova*, 2002]. Nonetheless, the locked source asperities of many such events and their associated stress shadows will further diminish the rate of aseismic slip that currently takes place on the plate interface.

[43] In the forward models, we simply placed the asperities in the central area of the previously proposed rupture zones. Of course, we have no direct knowledge of the actual location of asperities in these ruptures, with the exception of the 1952 earthquake. When comparing the model that considered only high-slip portions of the 1952 rupture (Figure 9c) with a simple reduction in the rupture extent to 25% (Figure 9f), we see that the details of the coseismic slip distribution and the criteria used to infer the existence of asperities may strongly influence the expected regional velocity field. As GPS precision and the station distribution improve, we will be able to better map the extent of actual asperity zones and thus greatly improve our understanding of the relationship between historic ruptures and currently locked portions of the fault plane.

[44] The overall success of a locking model that is defined by historic earthquake ruptures suggests that (1) the historic observations span the ruptures of most, if not all, major asperities and (2) that the location of locked asperities is a persistent feature at least over time spans of a single earthquake cycle. Some previous interseismic GPS studies also suggest an apparent correlation between historic coseismic slip regions and currently locked zones [*Sagiya*, 1999; *Freymueller et al.*, 2000]. Of course, this does not rule out that rupture characteristics change from event to event, as they break smaller or larger portions of the plate interface. This is illustrated by the 2004 Sumatra-Andaman earthquake, which apparently reruptured previous rupture zones of $M \approx 8$ earthquakes that occurred in 1881 and 1941. A detailed study of eight large ($M > 7$) earthquake ruptures off northeastern Japan over the past 70 years [*Yamanaka and Kikuchi*, 2004] suggests that asperities have repeatedly failed in a number of events, but that individual earthquakes may include a variable number of subasperities. While our analysis is overall consistent with the view that persistent asperities define the interseismic locking distribution along a subduction zone, the lack of a sufficiently extensive catalog of past ruptures and their detailed spatial extent and slip distribution does not allow us to address possible implications for the nature of future ruptures.

5.2. Factors in Spatial Variations of Coupling Along Kamchatka Subduction Zone

[45] In global analyses of great earthquake ruptures, *Wells et al.* [2003] and *Song and Simons* [2003] find a strong correlation of high-slip asperities with overlying forearc areas of relatively low free-air gravity anomaly and deep bathymetry. *Song and Simons* [2003] also find a significant correlation of the gravity and bathymetry variation with moment release in $M \geq 6$ subduction earthquakes. The forearc basins outlined by the gravity and bathymetric lows also tend to be associated with embayments along the coastline of both accretionary and nonaccretionary subduction zones. The strongest correlation appears to be between the areas lacking large earthquakes and regions of high gravity anomaly and bathymetry and associated peninsulas [*Song and Simons*, 2003]. *Wells et al.* [2003] suggest that the lack of seismic moment release beneath structural highs may be due to higher temperatures and fluid pressures in those locations, while the development of forearc basins may indicate a link between subsidence, subduction erosion, and the mechanical properties of the subduction thrust. *Song and Simons* [2003] favor a model in which variations in the frictional strength of the subduction thrust control the forearc structure and the distribution of seismic and aseismic moment release.

[46] Figure 7c shows a map of isostatic gravity anomalies in the region of the Kamchatka subduction zone derived from on-land gravimeter measurements [*Kogan et al.*, 1994] and satellite altimetry over the oceans [*Sandwell and Smith*, 1997]. The isostatic gravity high over the east coast of Kamchatka reflects the presence of the cold subducted slab and terminates about 120 km south of the Kamchatka-Aleutian subduction cusp. Variations in the gravity field along the subduction zone, often coincident with changes in the coastal morphology and topography are related to variable forearc structure. Along the Kuril-Kamchatka subduction zone an apparent 600-km-long gap in the occurrence of large earthquakes south of 49°N coincides with a region of relatively high gravity [*Song and Simons*, 2003]. The notable peninsulas along the Kamchatka coastline north of this seismic gap are the result of mid-Cretaceous to late Eocene terrane accretion [*Park et al.*, 2002] and lead to a significantly perturbed morphology and gravity field of the forearc. Where the Meiji seamounts (the northernmost extension of the Hawaii-Emperor seamount chain) encounter the subduction zone, gravity and bathymetric highs and the Kronotsky Peninsula are found. Subduction of the Kruzenstern fracture zone near 52.5°N also appears to perturb the forearc structure [*Gorbatov et al.*, 1997].

[47] The heterogeneous nature of the downgoing plate appears to correlate with the distribution of large historic earthquake ruptures. A number of the historic earthquakes along Kamchatka occurred below apparent forearc basins (e.g., 1841, 1917, 1923, 1971, and 1997); however, the source areas of the earlier events are not well determined. Neither *Wells et al.* [2003] nor *Song and Simons* [2003] found a good correlation of forearc bathymetry or free-air gravity anomaly and the areas of large (>6 m) coseismic slip of the 1952 earthquake determined by *Johnson and Satake*

[1999]. Specifically a 6–8 m high-slip patch of the 1952 source model lies directly over the gravity high offshore of Shipunsky peninsula. We find that the vigorous foreshock sequence of the 1997 Kronotsky earthquake that may have accompanied a precursory aseismic slip event [*Gordeev et al.*, 2001], occurred in an area of high gravity anomaly. The coseismic rupture broke from the epicenter southward into a region of relatively low gravity anomaly [*Bürgmann et al.*, 2001].

[48] Our study finds a comparable pattern to the distribution of coseismic rupture asperities in the distribution of aseismic slip we infer from the interseismic GPS velocities. Depending on the degree of smoothing chosen, the distributed slip model inversions indicate three or four distinct areas of locking or very slow slip that are roughly anticorrelated with gravity highs and the coastal peninsulas (Figure 7). The subduction thrust is inferred to be nonslipping just south of Kronotsky Peninsula including the rupture area of the 1997 earthquake and found to be uncoupled to the east of the Peninsula where no large historic events occurred. The highest kinematic coupling is inferred for the region just south of Shipunsky peninsula, which coincides in part with a strong negative gravity anomaly there, but also overlaps significantly with a gravity high and bathymetric ridge extending from the peninsula. We currently lack the resolution in our inversions to document a more detailed correlation of forearc basin structures and locked portions of the subduction thrust.

5.3. Implications for Time Variability of Aseismic Fault Slip

[49] Afterslip and transient slip events of varying size and duration have been documented along many of the world's subduction zones. In Kamchatka continuously operating GPS stations revealed a phase of rapidly decaying, transient afterslip, which over 40 days amounted to as much as the coseismic moment [*Bürgmann et al.*, 2001]. The temporal evolution of the transient deformation is consistent with afterslip on velocity-strengthening portions of the plate interface adjacent to the asperity that dynamically ruptured in the earthquake, but some of the afterslip might well have occurred on the coseismic rupture itself. The afterslip apparently includes a zone of vigorous foreshock activity located about 50 km to the north of the coseismic rupture, which may have been associated with slow slip preceding the main shock [*Gordeev et al.*, 2001]. Thus transient aseismic fault slip can account for a significant amount of plate interface slip along the partially coupled portion of the Kamchatka subduction zone and the kinematic coupling we document likely overestimates the seismic potential or seismic slip deficit. Some fault patches that are currently not slipping or slipping at a reduced rate may relieve stress by independent slow slip events of unknown duration or size.

6. Conclusions

[50] Our modeling of the interseismic deformation measured with GPS suggests that the Kamchatka subduction zone is characterized by persistent locked asperities that episodically slip in large earthquakes. Inversions for the distribution of slip on the subduction interface from the trench to 60-km depth suggest a mostly uncoupled subduction thrust north of $\sim 53^\circ$ latitude, while substantial slip deficits accumulate on the plate interface to the south, where the $M \approx 9$, 1952 earthquake occurred. Fully locked asperities appear to be much smaller than the associated rupture zones inferred from aftershock distributions, as models assuming full interseismic coupling of historic rupture zones are inconsistent with the geodetically measured velocity field. Thus major earthquakes also rupture surrounding portions of the plate interface that currently slip aseismically at low rates. The remaining, velocity strengthening plate interface accommodates aseismic slip interseismically and by accelerated afterslip following earthquakes. There is a first-order correlation between portions of the subduction thrust that are currently nonslipping, the rupture zones of large historic earthquakes, and regions of low gravity and bathymetry associated with forearc basin structure; however, this relationship is not without exceptions.

[51] **Acknowledgments.** This project would be impossible without the devoted work of members of GPS field teams in Kamchatka. We thank Kelin Wang, Paul Lundgren, and Jeff Freymueller for their helpful comments and reviews. Figures were drawn with the GMT software [*Wessel and Smith*, 1995]. This project is supported by the National Science Foundation under grants 0106002 to UCB, 0106999 to LDEO, and 0105587 to MIT, as well as a JPL grant 1203235 and an IRIS grant 311, both to LDEO. Berkeley Seismolab contribution 05-07.

References

Bogdanov, N. A., and V. E. Khain (2000), The Sea of Okhotsk region, tectonic map with explanatory notes, scale 1:250,000, 171 pp., Inst. of the Lithosphere of Marginal Seas, Russ. Acad. of Sci., Moscow.

Bürgmann, R., D. D. Pollard, and S. J. Martel (1994), Slip distribution on faults: Effects of stress gradients, inelastic deformation, heterogeneous host-rock stiffness, and fault interaction, *J. Struct. Geol.*, *16*, 1675–1690.

Bürgmann, R., P. Segall, M. Lisowski, and J. Svarc (1997), Postseismic strain following the 1989 Loma Prieta earthquake from GPS and leveling measurements, *J. Geophys. Res.*, *102*, 4933–4955.

Bürgmann, R., M. G. Kogan, V. E. Levin, C. H. Scholz, R. W. King, and G. M. Steblov (2001), Rapid aseismic moment release following the 5 December, 1997 Kronotsky, Kamchatka, earthquake, *Geophys. Res. Lett.*, *28*, 1331–1334.

Crouch, S. L., and A. M. Starfield (1983), *Boundary Element Methods in Solid Mechanics*, 322 pp., CRC Press, Boca Raton, Fla.

DeMets, C., R. G. Gordon, D. F. Argus, and S. Stein (1990), Current plate motions, *Geophys. J. Int.*, *101*, 425–478.

Dragert, H., W. Kelin, and T. S. James (2001), A silent slip event on the deeper Cascadia subduction interface, *Science*, *292*, 1525–1528.

Du, Y., A. Aydin, and P. Segall (1992), Comparison of various inversion techniques as applied to the determination of a geophysical deformation model for the 1983 Borah Peak earthquake, *Bull. Seismol. Soc. Am.*, *82*, 1840–1866.

Dziewonski, A. M., G. Ekström, and N. N. Maternovskaya (1998), Centroid-moment tensor solutions for October–December, 1997, *Phys. Earth Planet. Inter.*, *109*, 93–105.

Engdahl, E. R., R. D. van der Hilst, and R. P. Buland (1998), Global teleseismic earthquake relocation with improved travel times and procedures for depth determination, *Bull. Seismol. Soc. Am.*, *88*, 722–743.

Fedotov, S. A., S. D. Chernyshev, Y. D. Matvienko, and N. A. Zharinov (1999), The forecast of the December 5, 1997, magnitude 7.8–7.9 Kronotsky earthquake, Kamchatka, and its $M \geq 6$ aftershocks, *Volcanol. Seismol.*, *20*, 597–613.

Freymueller, J. T., and J. Beavan (1999), Absence of strain accumulation in the western Shumagin segment of the Alaska subduction zone, *Geophys. Res. Lett.*, *26*, 3233–3236.

Freymueller, J. T., R. Cohen, and H. Fletcher (2000), Spatial variations in present-day deformation, Kenai Peninsula, Alaska, and their implications, *J. Geophys. Res.*, *105*, 8079–8101.

Geist, E. L., and D. W. Scholl (1994), Large-scale deformation related to the collision of the Aleutian arc with Kamchatka, *Tectonics*, *13*, 538–560.

Gorbatov, A., V. Kostoglodov, G. Suárez, and E. Gordeev (1997), Seismicity and structure of the Kamchatka subduction zone, *J. Geophys. Res.*, *102*, 17,883–17,898.

Gordeev, E., V. Levin, M. Kasahara, V. Bakhtiarov, V. Chebrov, and M. Maguskin (1999), GPS monitoring in Kuril-Kamchatka and Aleutian arcs junction, *Eos Trans. AGU*, *80*(46), 948.

Gordeev, E., A. A. Gusev, V. E. Levin, V. F. Bakhtiarov, V. M. Pavlov, V. N. Chebrov, and M. Kasahara (2001), Preliminary analysis of deformation at the Eurasia-Pacific-North America plate junction from GPS data, *Geophys. J. Int.*, *147*, 189–198.

Harris, R., and P. Segall (1987), Detection of a locked zone at depth on the Parkfield, California segment of the San Andreas fault, *J. Geophys. Res.*, *92*, 7945–7962.

Heki, K., S. Miyazaki, and H. Tsuji (1997), Silent fault slip following an interplate thrust earthquake at the Japan trench, *Nature*, *386*, 595–598.

Herring, T. A. (2002), GLOBK, Global Kalman filter VLBI and GPS analysis program, version 10.0, Mass. Inst. of Technol., Cambridge.

Hirose, J., K. Hirahara, F. Kimata, N. Fujii, and S. Miyazaki (1999), A slow thrust slip event following the two 1996 Hyuganada earthquakes beneath the Bongo Channel, southwest Japan, *Geophys. Res. Lett.*, *26*, 3237–3240.

Johnson, J. M., and K. Satake (1999), Asperity distribution of the 1952 great Kamchatka earthquake and its relation to future earthquake potential in Kamchatka, *Pure Appl. Geophys.*, *154*, 541–553.

King, R. W., and Y. Bock (2002), Documentation for the GAMIT GPPS analysis software, release 10.0, Mass. Inst. of Technol., Cambridge, 15 Feb.

Kogan, M. G., J. D. Fairhead, G. Balmino, and E. L. Makedonskii (1994), Tectonic fabric and lithospheric strength of northern Eurasia based on gravity data, *Geophys. Res. Lett.*, *21*, 2653–2656.

Lay, T., and H. Kanamori (1981), An asperity model of great earthquake sequences, in *Earthquake Prediction: An International Review*, *Maurice Ewing Ser.*, vol. 4, edited by D. W. Simpson and P. G. Richards, pp. 579–592, AGU, Washington, D. C.

Lay, T., and S. Y. Schwartz (2004), Comment on "Coupling semantics and science in earthquake research," *Eos Trans. AGU*, *85*(36), 339–340.

Levin, V., J. Park, M. Brandon, J. Lees, V. Peyton, E. Gordeev, and A. Ozerov (2002a), Crust and upper mantle of Kamchatka from teleseismic receiver functions, *Tectonophysics*, *358*(1–4), 233–265.

Levin, V., N. Shapiro, J. Park, and M. H. Ritzwoller (2002b), Seismic evidence for catastrophic slab loss beneath Kamchatka, *Nature*, *418*, 763–766.

Lundgren, P., M. Protti, A. Donnellan, M. Heflin, E. Hernandez, and D. Jefferson (1999), Seismic cycle and plate margin deformation in Costa Rica: GPS observations from 1994 to 1997, *J. Geophys. Res.*, *104*, 28,915–28,926.

Lutikov, A. I., and G. U. Dontsova (2002), Estimation of linear dimensions of Kamchatka earthquake sources from the dimensions of the aftershock region, *Izv. Phys. Solid Earth*, *38*(6), 485–495.

Mazzotti, S., X. Le Pichon, and P. Henry (2000), Full interseismic locking of the Nankai and Japan-west Kurile subduction zones: An analysis of uniform elastic strain accumulation in Japan constrained by permanent GPS, *J. Geophys. Res.*, *105*, 13,159–13,177.

Miller, M. M., T. Melbourne, D. J. Johnson, and W. Q. Sumner (2002), Periodic slow earthquakes from the Cascadia subduction zone, *Science*, *295*, 2423.

Miyazaki, S., P. Segall, J. Fukuda, and T. Kato (2004), Space-time distribution of afterslip following the 2003 Tokachi-oki earthquake: Implications for variations in fault zone frictional properties, *Geophys. Res. Lett.*, *31*, L06623, doi:10.1029/2003GL019410.

Okada, T., K. Sakoda, T. Matsuzawa, R. Hino, A. Hasegawa, S. Sakai, and T. Kanazawa (2004), Characteristic seismic activity in the subducting plate boundary zone off Kamaishi, northeastern Japan, revealed by precise hypocenter distribution analysis using ocean-bottom seismometers, *Geophys. Res. Lett.*, *31*, L19604, doi:10.1029/2004GL020366.

Okada, Y. (1985), Surface deformation due to shear and tensile faults in a half-space, *Bull. Seismol. Soc. Am.*, *75*, 1135–1154.

Oleskevich, D., R. D. Hyndman, and K. Wang (1999), The updip and downdip limits of subduction earthquakes: Thermal and structural models of Cascadia, south Alaska, S.W. Japan, and Chile, *J. Geophys. Res.*, *104*, 14,965–14,991.

Pacheco, J. F., L. R. Sykes, and C. H. Scholz (1993), Nature of seismic coupling along simple plate boundaries of the subduction type, *J. Geophys. Res.*, *98*, 14,133–14,159.

Park, J., V. Levin, M. Brandon, J. Lees, V. Peyton, E. Gordeev, and A. Ozerov (2002), A dangling slab, amplified arc volcanism, mantle flow and seismic anisotropy in the Kamchatka plate corner, in *Plate Boundary Zones*, *Geodyn. Ser.*, vol. 30, edited by S. Stein and J. T. Freymueller, pp. 295–324, AGU, Washington, D. C.

Price, E. J., and R. Bürgmann (2002), Interactions between the Landers and Hector Mine earthquakes from space geodesy, boundary element modeling, and time-dependent friction, *Bull. Seismol. Soc. Am.*, *92*, 1450–1469.

Sagiya, T. (1999), Interplate coupling in the Tokai district, central Japan, deduced from continuous GPS data, *Geophys. Res. Lett.*, *26*, 2315–2318.

Sandwell, D., and W. H. F. Smith (1997), Marine gravity anomaly from Geosat and ERS 1 satellite altimetry, *J. Geophys. Res.*, *102*, 10,039–10,054.

Savage, J. C. (1983), A dislocation model of strain accumulation and release at a subduction zone, *J. Geophys. Res.*, *88*, 4984–4996.

Schmidt, D. A., R. Bürgmann, R. M. Nadeau, and M. A. d'Alessio (2005), Distribution of aseismic slip rate on the Hayward fault inferred from seismic and geodetic data, *J. Geophys. Res.*, doi:10.1029/2004JB003397, in press.

Scholz, C. H. (1998), Earthquakes and friction laws, *Nature*, *391*, 37–42.

Seno, T., T. Sakurai, and S. Stein (1996), Can the Okhotsk plate be discriminated from the North American plate?, *J. Geophys. Res.*, *101*, 11,305–11,315.

Simoes, M., J. P. Avouac, R. Cattin, and P. Henry (2004), The Sumatra subduction zone: A case for a locked fault zone extending into the mantle, *J. Geophys. Res.*, *109*, B10402, doi:10.1029/2003JB002958.

Sohn, S. W. (1998), The 1997 Kamchatka earthquake, in *Individual Studies by Participants at the International Institute of Seismology and Earthquake Engineering*, vol. 34, pp. 91–99, Int. Inst. of Seismol. and Earthquake Eng., Tokyo.

Song, T.-R. A., and M. Simons (2003), Large trench-parallel gravity variations predict seismogenic behaviour in subduction zones, *Science*, *301*, 630–633.

Stark, P. B., and R. L. Parker (1995), Bounded variable least squares: An algorithm and applications, *Comput. Stat.*, *10*, 129–141.

Steblov, G. M., M. G. Kogan, R. W. King, C. H. Scholz, R. Bürgmann, and D. I. Frolov (2003), Imprint of the North American plate in Siberia revealed by GPS, *Geophys. Res. Lett.*, *30*(18), 1924, doi:10.1029/2003GL017805.

Thomas, A. L. (1993), Poly3D: A three-dimensional, polygonal element, displacement discontinuity boundary element computer program with applications to fractures, faults, and cavities in the Earth's crust, M.S. thesis, 221 pp., Stanford Univ., Stanford, Calif.

Tibaldi, A. (2004), International team investigates large recent surface faulting in the Kamchatka volcanic arc, far eastern Russia, *Eos Trans. AGU*, *85*(14), 133.

Tichelaar, B. W., and L. J. Ruff (1993), Depth of seismic coupling along subduction zones, *J. Geophys. Res.*, *98*, 2017–2037.

Wang, K., and T. H. Dixon (2004), "Coupling" semantics and science in earthquake research, *Eos Trans. AGU*, *85*(18), 180.

Wells, R. E., R. J. Blakely, Y. Sugiyama, D. W. Scholl, and P. A. Dinterman (2003), Basin-centered asperities in great subduction zone earthquakes: A link between slip, subsidence, and subduction erosion?, *J. Geophys. Res.*, *108*(B10), 2507, doi:10.1029/2002JB002072.

Wessel, P., and W. H. F. Smith (1995), New version of the Generic Mapping Tools released, *Eos Trans. AGU*, *76*, 329.

Yagi, Y., M. Kikuchi, and T. Nishimura (2003), Co-seismic slip, post-seismic slip, and largest aftershock associated with the 1994 Sanriku-haruka-oki, Japan, earthquake, *Geophys. Res. Lett.*, *30*(22), 2177, doi:10.1029/2003GL018189.

Yamanaka, Y., and M. Kikuchi (2004), Asperity map along the subduction zone in northeastern Japan inferred from regional seismic data, *J. Geophys. Res.*, *109*, B07307, doi:10.1029/2003JB002683.

Zobin, V. M., and V. I. Levina (2001), The rupture process of the Mw 7.8 Cape Kronotsky, Kamchatka, earthquake of 5 December 1997 and its relationship to foreshocks and aftershocks, *Bull. Seismol. Soc. Am.*, *91*, 1619–1628.

E. Apel and R. Bürgmann, Department of Earth and Planetary Science, University of California, Berkeley, CA 94720, USA. (burgmann@seismo.berkeley.edu)

G. Hilley, Department of Geological and Environmental Sciences, Stanford University, Stanford, CA 94305, USA.

M. G. Kogan, Lamont-Doherty Earth Observatory, Palisades, NY 10964-1000, USA.

V. E. Levin, KOMSP, GSRAS, Petropavlovsk 683006, Russia.

G. M. Steblov, RDAAC, GSRAS, Moscow 117333, Russia.